



Modelling of heat conduction calorimeters. Case of a non-differential skin calorimeter

Pedro Jesús Rodríguez de Rivera^{a,*}, Miriam Rodríguez de Rivera^b, Fabiola Socorro^a, Manuel Rodríguez de Rivera^a

^a Department of Physics, University of Las Palmas de Gran Canaria, Las Palmas de Gran Canaria, Campus de Tafira E-35017, Spain

^b Cardiology Service, Hospital Universitario Marqués de Valdecilla, E-39008 Santander, Spain

ARTICLE INFO

Keywords:

Conduction calorimetry
Non-differential calorimeter
Skin heat flux
Skin calorimeter
Skin thermal properties
Sports medicine sensors

ABSTRACT

In non-differential calorimeters, the ambient temperature, the thermostat temperature, and the thermostat cooling system affect the measured heat flux. For this reason, the modelling and calibration procedures should take into account all the variables that affect the heat flux transmitted through the calorimeter. In this work, we present the complete calibration of three non-differential skin calorimeters designed to measure the heat flux, the heat capacity and the thermal resistance of a localized skin surface. In addition, the incorporation of the skin into the calorimetric model allows the determination of the core temperature of the tissue where the measurement is performed. The electrical calibration is validated with measurements with the three calorimeters on the volar and dorsal areas of the wrist of a healthy 30-year-old male subject.

1. Introduction

Nowadays, calorimetry is an essential technique for measuring the energy or the power developed in any thermal process, as well as for determining the thermal properties of materials [1]. The technology used depends on the process under study (e.g., liquid-liquid, solid-gas, liquid-gas, etc.) and adaptations are required for each case. However, all calorimeters share a common characteristic: the process is performed in a purpose-built environment under controlled conditions of pressure and temperature. Hansen [2] proposes a classification of calorimeters according to the method of operation and other characteristics.

The skin calorimeters presented in this work are applied on the skin, and their principle of operation involves measuring the heat flux transmitted by conduction from the skin to the calorimeter. This measurement allows the determination of the thermal properties of the localized human skin region [3]. In Hansen's classification, these instruments are included in the group of heat conduction calorimeters [2].

Two types of models are commonly used in heat conduction calorimeters: 1) empirical input-output models defined by a transfer function (TF models) [4], and 2) models derived from decomposing the calorimeter into different domains connected by thermal couplings (RC models) [5]. The parameters of both TF and RC models can be related, since it is the same instrument and share the same input and output

signals. TF models are mainly used in isothermal calorimeters whose purpose is to determine the energy or the power developed in a thermal process. However, when there are factors that can modify the Transfer Function, the RC models are used instead because these effects can be easily incorporated. For example, in flow calorimeters, the effect of liquid injection must be included in the equations [6]. In titration calorimeters, in addition to the effect of liquid injection, the rise in the liquid level inside the measuring cell alters the conductances between the cell and the neighbouring domains. This produces calorimetric signal changes that can be assessed through these RC models [7].

The conduction heat transfer process is also modelled with the differential form of the Fourier equation [8]. Additional phenomena can be incorporated into this equation, for example, the blood perfusion process in the case of skin [9]. The integration in each domain can be carried out with the finite element method (FEM) using the boundary conditions between domains. Several works have been conducted to study the spatiotemporal evolution of temperature in materials [10]. This method is not the most appropriate for modelling the operation of a calorimeter, since these instruments are designed to provide a direct and simple relationship between the variables measured and the thermal quantities to be measured. However, calorimetric results (heat capacity and thermal conductivity of materials) are indispensable in thermal FEM modelling.

* Corresponding author at: Department of Physics, University of Las Palmas de Gran Canaria, Las Palmas de Gran Canaria, Spain.

E-mail address: pedro.riguezderivera@ulpgc.es (P.J. Rodríguez de Rivera).

<https://doi.org/10.1016/j.tca.2025.180015>

Received 22 March 2025; Received in revised form 20 April 2025; Accepted 21 April 2025

Available online 21 April 2025

0040-6031/© 2025 The Authors. Published by Elsevier B.V. This is an open access article under the CC BY license (<http://creativecommons.org/licenses/by/4.0/>).

Heat conduction calorimeters typically operate in a differential setup, using two identical cells. One cell contains the thermal process under study, while the other is used as a reference. This differential setup prevents the measurement baseline from being affected by the variation of the thermostat and the ambient temperature. However, the skin calorimeter presented in this work is non-differential, so the variations of the ambient and the thermostat temperature affect the measured signals. For this reason, a specific modelling for these skin calorimeters is necessary. This is the main objective of this paper. This study is also highly relevant for the development of other calorimetric devices that, due to their specific applications, must operate as non-differential systems [11]. In this work, we propose a model that takes into account the external temperatures of the calorimeter and incorporates the internal thermal resistance of the skin. The model allows quantifying all heat fluxes through the calorimeter, without baseline correction. In addition, the incorporation of the thermal resistance of the skin allows to determine the internal temperature in the area where the measurement is made. Thus, this work is a clear advance over previous work in which the calorimetric model related the calorimetric variables after a baseline correction to an initial steady state [12].

This skin calorimeter has two main functions. First, it is used to determine the thermal resistance and the heat capacity of a localized skin area. These parameters have been used to monitor the short-term recovery of minor skin injuries through daily measurements [13]. Second, it measures the skin heat flux at the studied region, both when the subject is at rest or performing physical exercise. In all cases, these calorimeters are attached to the skin using an adapted holding system. Having outlined the problem to be addressed, we first describe the experimental system and the operating model. This is followed by a detailed study of the calibration process of three similar skin calorimeters. Finally, some applications on human skin are presented.

2. Experimental system

2.1. Skin calorimeter

The skin calorimeters presented in this work are based on a measuring thermopile ($13.2 \times 13.2 \times 2.2$ mm) placed between an aluminum measuring plate ($20 \times 20 \times 1$ mm) and an aluminum thermostat ($14 \times 14 \times 4$ mm). The thermostat contains a PT-100 temperature sensor and a heating resistor. This thermostat incorporates a cooling system based on another thermopile, a heatsink and a fan (see Fig. 1).

Three prototypes with a measuring area of 2×2 cm² have been built; the first one (S0) in 2016 and the others (S1 and S2) in 2024 [3]. The main difference between these prototypes lies in the thermopiles and the heatsink used. The differences are clearly reflected in the calibration results. S1 and S2 calorimeters have more sensitive thermopiles and a wider operating range (programmable thermostat temperature)

compared to the S0 calorimeter. For each experimental setup, we built a calibration base with an electrical heating resistor. Thermopiles are from Laird Thermal Systems [14]. The PT-100 temperature sensor and the constantan wire used to build the calibration base and thermostat resistors are from Omega Engineering [15].

2.2. calorimetric model and operating diagram

We use a common approach for the modelling of calorimeters [5]. This approach, called RC model, consists of decomposing the experimental system into N domains of heat capacity C_i , connected to the other domains by thermal couplings of conductance P_{ik} . Each domain is assumed to have infinite thermal conductivity, so the temperature at all points in that domain can be considered the same. Under this assumption, the power developed in each domain (W_i) is equal to the power required to change its temperature ($C_i dT_i / dt$) plus the sum of the conduction losses to the other domains, including the heat losses to the outside of the calorimeter (T_{0i}). In conduction calorimeters, the thermal process under study occurs in the measuring zone. This zone is covered by a thermostat whose temperature is known and well controlled.

The number of N domains is directly related to the signal-to-noise ratio of the measured signals. In practice, N is determined from preliminary calibration measurements that allow the determination of the minimum number of poles of a Transfer Function that is able to reproduce the calorimetric signal provided by the measuring thermopile (output signal) from a known power that passes through the measuring thermopile (input signal). This input power is dissipated by an electrical calibration resistor.

In our calorimeters, we have found that a two-pole Transfer Function is enough to reproduce the behavior of the system. Thus, we decompose the calorimeter into two domains. The first one represents the heat source, the measuring plate and the layer of the thermopile that contacts this measuring plate. When the calorimeter is placed on the calibration base, the power dissipated in this domain is the power dissipated in the calibration resistor W_1 . The second domain represents the thermostat and the layer of the thermopile in contact with the thermostat. In this domain, W_2 is the power dissipated in the heating resistor located in the thermostat, whose purpose is to maintain the programmed temperature T_2 . Thus, the system of equations will be as follows:

$$\begin{aligned} W_1 &= C_1 \frac{dT_1}{dt} + P_{12}(T_1 - T_2) + P_1(T_1 - T_{01}) \\ W_2 &= C_2 \frac{dT_2}{dt} + P_{12}(T_2 - T_1) + P_2(T_2 - T_{02}) \end{aligned} \quad (1)$$

The heat capacities of the domains are C_1 and C_2 . P_{12} is the thermal conductance of the measurement thermopile, which thermally connects the two domains. P_1 is the thermal conductance between the first domain and the environment, which is at a temperature T_{01} , and P_2 is

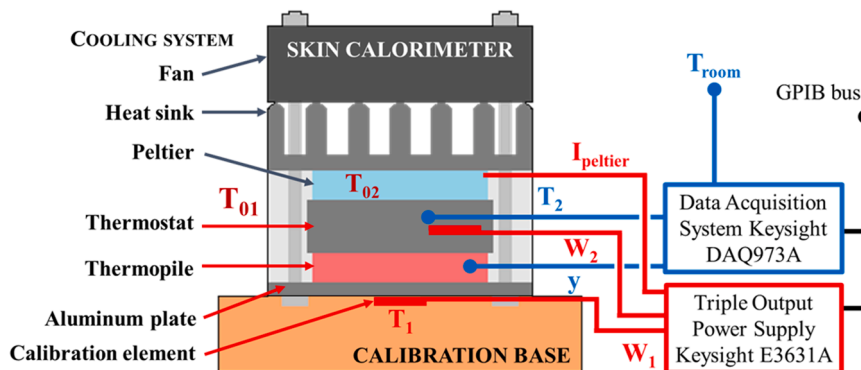


Fig. 1. Skin calorimeter scheme. Temperatures: ambient (T_{room}), thermostat (T_2), measurement plate (T_1), external (T_{01}), and cold focus (T_{02}). Calorimetric signal (y), heating powers (W_1 , W_2), and Peltier current (I_{pel}).

the thermal conductance between the thermostat and the cooling system, which is at a temperature T_{02} . We assume that the calorimetric signal provided by the measuring thermopile is linearly related to the temperature difference between the two domains, through the Seebeck coefficient:

$$y = k(T_1 - T_2) \quad (2)$$

By solving Eq. (2) for T_1 and substituting it into Eq. (1), we obtain the system of equations (Eq. (3)) which represents the calorimetric model and relates the input powers $W_1(t)$ and $W_2(t)$ with the output signals $y(t)$ and $T_2(t)$.

$$W_1 = \frac{C_1}{k} \frac{dy}{dt} + \frac{P_1 + P_{12}}{k} y + C_1 \frac{dT_2}{dt} + P_1(T_2 - T_{01}) \quad (3)$$

$$W_2 = -\frac{P_{12}}{k} y + C_2 \frac{dT_2}{dt} + P_2(T_2 - T_{02})$$

Fig. 2 shows a diagram of the skin calorimeter operation principle. The cooling system modifies the temperatures outside the calorimeter. The temperature T_{02} of the side of the cooling thermopile in contact with the thermostat is reduced by Peltier effect, as a function of the supply current I_{pel} . This causes a temperature increase on the other cooling thermopile side, which has to be cooled by the heatsink and the fan, causing the outside temperature T_{01} to rise slightly. Thus, the external temperatures T_{01} and T_{02} will depend on the ambient temperature T_{room} and the current I_{pel} . When the skin calorimeter is placed on the calibration base, the power W_1 is the power dissipated by the calibration resistor. But when the calorimeter is applied on the skin, W_1 is the heat flux transmitted by conduction from the skin. The power W_2 is determined by a PID controller [16] to achieve the set thermostat temperature T_{2REF} . The calorimetric signal y , the room and thermostat temperatures T_{room} & T_2 , are acquired with a Data Acquisition System (Keysight 34970A & 34901A). The cooling thermopile supply current I_{pel} , the power dissipated in the calibration base W_1 , and in the thermostat W_2 , are provided by a triple programmable power supply (Keysight E3631A). The acquisition program is written in C++ and controls the instruments via the GPIB bus (Keysight 82357B), with a sampling period of $\Delta t = 1$ s (see Fig. 1).

3. Calibration

3.1. Experimental calibration measurements

To identify the calorimetric model, we conducted measurements for different values of the thermostat temperature T_2 , the power dissipated in the calibration base W_1 , and the cooling thermopile supply current I_{pel} . The selected values represent an appropriate order of magnitude for human skin applications. Fig. 3 shows an experimental measurement in which the thermostat temperature (T_2) is initially set at 28 °C. Once steady state is reached, the temperature is increased to 33 °C,

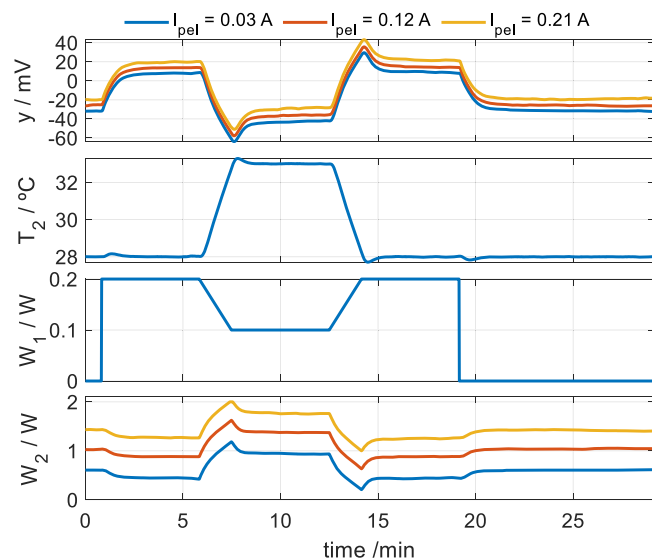


Fig. 3. Calibration measurement with variation of thermostat temperature (T_2) and calibration base power (W_1). The calorimetric signal (y) and the power dissipated in the thermostat (W_2) for the cases of cooling thermopile current (I_{pel}) of 0.03, 0.12 and 0.21 A are shown. Calorimeter S1 ($T_{room} = 21.2$ °C).

maintained for 5 min, and then lowered back to the initial value of 28 °C, at a heating/cooling rate of 3 K/min. Simultaneously, a power of $W_1 = 200$ mW is dissipated at the calibration base. This power decreases to 100 mW when the thermostat temperature increases, then returns to 200 mW, and finally, is stopped. This measurement is repeated for I_{pel} currents values: 0.03, 0.06, 0.09, 0.12, 0.15, 0.18, and 0.21 A. In Fig. 3, 0.03, 0.12 and 0.21 A cases are shown. In these measurements, we can observe the dependency of the calorimetric signal and the thermostat power on the I_{pel} value used.

3.2. Calibration with baseline correction

Calibration measurements are programmed to ensure that the initial and final steady states are identical. This is possible because the ambient temperature is essentially constant during the measurement time, and the cooling system's supply current (I_{pel}) is constant. Therefore, we can assume that the reference temperatures T_{01} and T_{02} are constant in that measurement. Under this conditions, we correct the baselines of the signals and obtain the system of equations (5), which relates the variation of the calorimetric signal Δy with the variation of the thermostat temperature ΔT_2 and the input powers variations ΔW_1 and ΔW_2 .

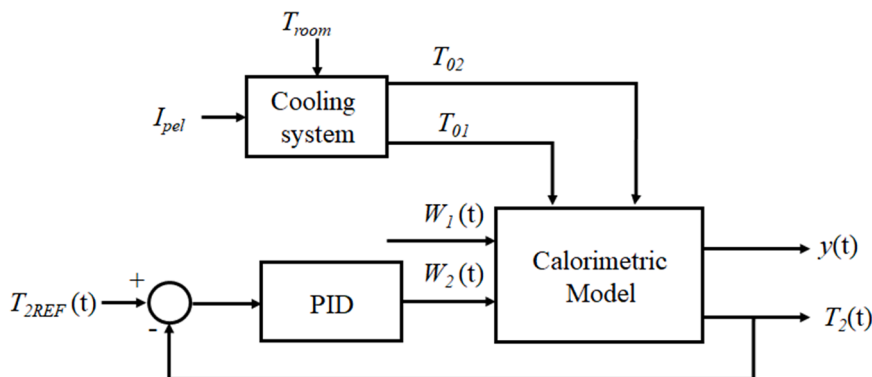


Fig. 2. Skin calorimeter operating diagram.

$$\Delta W_1 = \frac{C_1}{k} \frac{d\Delta y}{dt} + \frac{P_1 + P_{12}}{k} \Delta y + C_1 \frac{d\Delta T_2}{dt} + P_1 \Delta T_2$$

$$\Delta W_2 = -\frac{P_{12}}{k} \Delta y + C_2 \frac{d\Delta T_2}{dt} + P_2 \Delta T_2$$
(4)

The calibration process consists of determining the parameters C_1 , C_2 , P_1 , P_2 , P_{12} and k of the proposed model (Eq. (4)), using an iterative algorithm. From the known input powers W_1 and W_2 and the model parameters obtained in each iteration, the output variables Δy and ΔT_2 are determined. The identification process consists of an error minimization method based on the Nelder-Mead simplex algorithm [17] developed by Langarias et al. [18], and implemented in MatLab's `fminsearch` function [19]. The criterion to be minimized is the root mean squared error (RMSE) between the experimental curves (*exp* subscript) and the calculated ones (*cal* subscript):

$$\epsilon = \epsilon_y + \epsilon_{T_2}$$

$$= \frac{1}{np} \sqrt{\sum_{i=1}^{np} (y_{\text{exp}}(i) - y_{\text{cal}}(i))^2} + \frac{1}{np} \sqrt{\sum_{i=1}^{np} (T_{2\text{exp}}(i) - T_{2\text{cal}}(i))^2}$$
(5)

In this expression, ϵ_y and ϵ_{T_2} are the RMSE of the calorimetric signal (y) and the thermostat temperature (T_2), and np is the number of record points used. Fig. 4 shows the fit between the experimental and model-calculated curves in a calibration measurement, with the corresponding RMSE values indicated. Table 1 shows the results of this first step in the calorimeter calibration. Note that all model parameters are invariant except C_1 , which depends on the heat capacity of the heat source.

As mentioned above, these skin calorimeters are used in two applications. In the first one, heat capacity and thermal resistance of a localized skin area can be determined by programming a thermostat temperature variation. This requires knowing all the parameters of the calorimetric model. In a second application, the thermostat is set to a constant temperature to monitor heat flux variations (ΔW_1) in a specific skin area during rest or physical exercise. In this case, if the power ΔW_1 does not significantly affect the temperature of the thermostat, we can define a *TF* that allows us to compare different calorimeters and heat flux sensors. This *TF* is derived from the first equation (for constant T_2 value) of the system (5) and is defined by the equation:

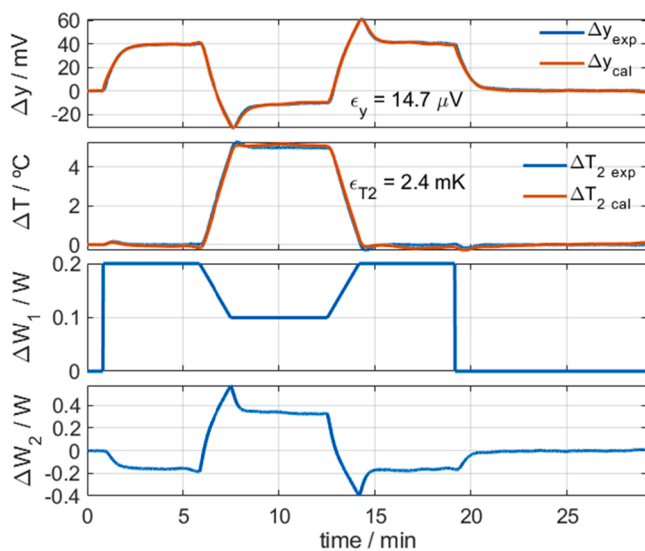


Fig. 4. Identification process, having corrected the baselines, for calorimeter *S1*, $I_{\text{pel}} = 0.03$ A and $T_{\text{room}} = 21.2$ °C. Calorimetric signal (Δy), thermostat temperature (ΔT_2), calibration base power (ΔW_1) and thermostat power (ΔW_2). Experimental curves (in blue) and model-calculated curves (in red). RMSE of each signal is indicated (Eq. (5)).

Table 1

Calibration results by correcting the baselines. RC model for *S0*, *S1* and *S2* skin calorimeters. Number of measurements = 35. Number of points for each measurement = 1750. Sampling period = 1 s. Average value (*Mean*) and standard deviation (*Std*). RMSE: ϵ_y & ϵ_{T_2} (Eq. (5)).

	<i>S0</i>		<i>S1</i>		<i>S2</i>		units
	Mean	Std	Mean	Std	Mean	Std	
C_1	3.960	0.060	4.020	0.090	3.910	0.090	J/K
C_2	4.800	0.100	3.800	0.200	3.700	0.300	J/K
P_1	0.033	0.001	0.029	0.002	0.029	0.002	W/K
P_2	0.053	0.002	0.057	0.005	0.055	0.005	W/K
P_{12}	0.128	0.005	0.092	0.008	0.089	0.009	W/K
k	23.10	0.500	23.70	1.100	23.00	1.400	mV/K
ϵ_y	14.10	0.800	16.50	2.500	16.20	2.400	μV
ϵ_{T_2}	4.300	0.600	3.900	2.000	3.800	2.000	mK

$$TF(s) = \frac{\Delta Y(s)}{\Delta W_1(s)} = \frac{k/(P_1 + P_{12})}{1 + sC_1/(P_1 + P_{12})} = \frac{K}{1 + s\tau}$$
(6)

Table 2 presents the sensitivity (K) and time constant (τ) for each calorimeter. Although the calorimeters are similar, *S1* and *S2* exhibit higher sensitivities than *S0* (+35 %) and higher time constants (+32 %).

3.3. Calibration without baseline correction

The calibration method described in Section 3.2 allows the determination of the heat flux variation in a given area, as the model relates power variations (ΔW_1 and ΔW_2) to calorimetric signal (Δy) and thermostat temperature variations (ΔT_2). However, this model does not provide the heat flux values at the initial and final states. To address this limitation, the external temperatures T_{01} and T_{02} from the model equation (Eq. (1)) must be known. For this purpose, we define the parameters ΔT_{01} and ΔT_{02} :

$$\Delta T_{01} = T_{01} - T_{\text{room}}$$

$$\Delta T_{02} = T_{02} - T_{\text{room}}$$
(7)

Now, for each calibration measurement, these parameters (ΔT_{01} and ΔT_{02}) are determined, while maintaining the parameters of the previously determined RC model (Table 1). For this purpose, we adopt the error minimization algorithm used previously [17–19]. Then, the calculated calorimetric signal and thermostat temperature curves are determined with the full calorimetric model given by Eq. (1), incorporating Eq. (7).

Fig. 5. illustrates an example of this calibration process, showing the fit between the experimental curves and those calculated by the model. The RMSE of the fit are also provided. Fig. 6. presents the values of the parameters ΔT_{01} and ΔT_{02} as a function of the cooling thermopile supply current (I_{pel}). Table 3 shows the coefficients of the linear fit for each skin calorimeter.

$$\Delta T_{01} = T_0 + \alpha I_{\text{pel}}$$

$$\Delta T_{02} = T_0 + \beta I_{\text{pel}}$$
(8)

An analysis of the results shows that skin calorimeters *S1* and *S2* dissipate the heat flux from the hot side of the cooling thermopile better than *S0* calorimeter. Additionally, *S1* and *S2* have a wider operating temperature range than *S0*, as they can reach lower cooling temperatures ($\Delta T_{02} = -19$ °C) compared to *S0* ($\Delta T_{02} = -9$ °C). It is important to note that the parameter T_0 (Eq. (8)) has been determined for the case in

Table 2

TF model of the studied calorimeters, for a constant thermostat temperature (Eq. (6)).

Skin calorimeters		<i>S0</i>	<i>S1</i>	<i>S2</i>	Units
Sensitivity	K	144	196	194	mV/W
Time constant	τ	25	33	33	s

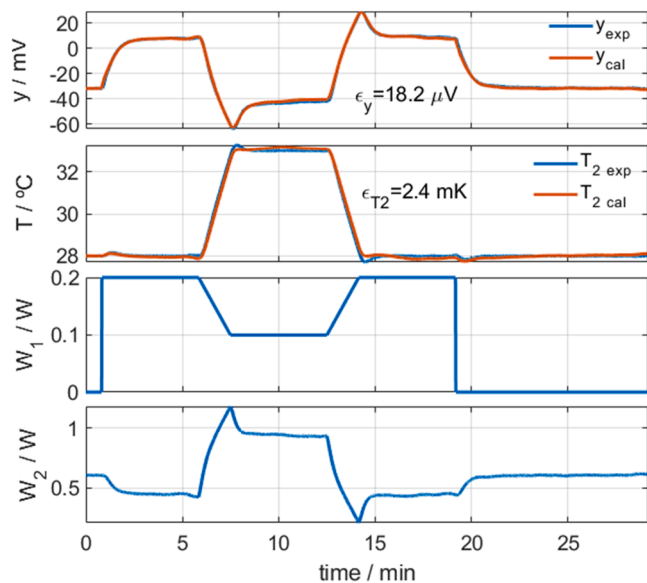


Fig. 5. Calibration measurement without baseline correction to determine the parameters ΔT_{O1} and ΔT_{O2} . Calorimetric signal (y), thermostat temperature (T_2), calibration base power (W_1) and thermostat power (W_2). Experimental curves (in blue) and model-calculated curves (in red) are plotted, indicating the RMSE of the fit (Eq. (5)). Case of calorimeter S1 with $I_{pel} = 0.03$ A, $T_{room} = 21.2$ °C.

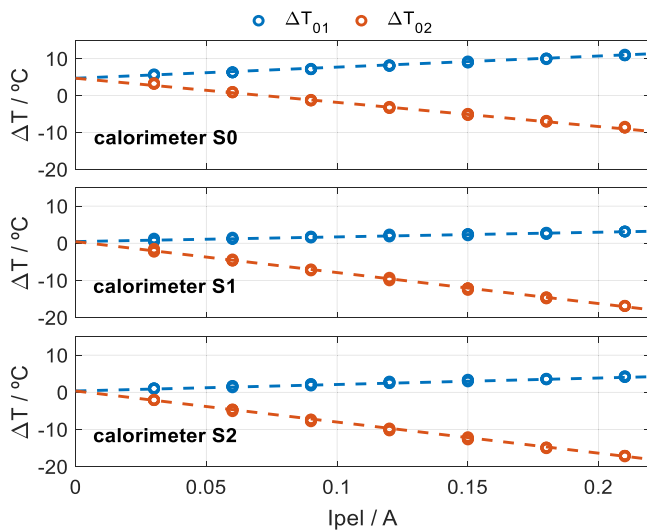


Fig. 6. Representation of ΔT_{O1} (in blue) and ΔT_{O2} (in red) (Eq. (10)) obtained from the calibration as a function of the cooling system supply current I_{pel} .

Table 3

Coefficients of the linear fit of the parameters ΔT_{O1} and ΔT_{O2} (see Fig. 6). Pearson coefficient r , number of points, np . Cooling system supply current I_{pel} in amperes (A).

	$\Delta T_{O1} = T_0 + \alpha I_{pel}$			$\Delta T_{O2} = T_0 + \beta I_{pel}$			np
	T_0 (°C)	α (°C/A)	r	T_0 (°C)	β (°C/A)	r	
S0	4.65	30.5	0.997	4.65	-65.2	-0.998	35
S1	0.45	13.6	0.971	0.45	-83.5	-0.999	35
S2	0.36	17.4	0.989	0.36	-83.8	-0.999	35

which the calorimeters are placed on a calibration base. When calorimeters are applied on the skin, T_0 increases due to the heating effect caused by proximity to the human body. Therefore, this parameter will

be determined in each measurement.

4. Application measurements on human body

In calorimetry, electrical calibration is always followed by measurements of a well-known thermal process that is used as a reference [20]. In the field of human heat dissipation, global heat loss measurements under different conditions are available. These measurements are used for designing thermal conditioning systems [21] and for assessing physical activity in healthy individuals or cardiac patients [22,23]. However, there are no standardized local heat dissipation measurements that can be used as a reference for different skin areas, as the available data vary significantly and lacked consensus over the past 50 years [3, 24–29]. Skin heat flux is highly variable, as it depends on the temperature of the calorimeter thermostat, as well as on the physical conditions of the subject and the environment. However, certain thermal parameters of the skin remain in a limited range of values, with temperature being the most relevant. In this paper, we also focus on the heat capacity and the equivalent thermal resistance of the skin. To determine these parameters, the calorimeter is applied on the skin. When the signals become stationary, the thermostat temperature is changed, and the calorimetric response is recorded. The dorsal and volar areas of the wrist were chosen for the study, as they are accessible and easy to measure. Repeated measurements have shown that the thermal resistance is generally higher in the volar region than in the dorsal zone [30].

4.1. Determination of heat capacity C_1 and power W_1

To determine the skin heat capacity C_1 , it is necessary to induce a thermal excitation on the skin and analyze the transient response of the calorimeter. This excitation is performed by varying the temperature of the calorimeter's thermostat, that produces a variation of the skin heat flux W_1 . Assuming that W_1 decreases as the thermostat temperature T_2 increases, according to the expression given in Eq. (9), both the skin heat flux W_1 and the skin heat capacity C_1 can be determined.

$$W_1(t) = W_{10} - \Delta W_1 \frac{T_2(t) - T_2(0)}{\Delta T_2} \quad (9)$$

In this equation, $T_2(t)$ is the programmed thermostat temperature, $T_2(0)$ is the initial stationary value and ΔT_2 is the maximum difference of the thermostat temperature. W_{10} is the initial stationary heat flux for $T_2(0)$, and ΔW_1 is the heat flux variation produced by the variation of ΔT_2 .

Using the model equations (Eq. (3)), we can find the values of C_1 and W_1 that accurately reproduce the calorimetric signal y and the thermostat temperature T_2 , using an error minimization algorithm similar to the one used previously [17–19]. In this case, the RC model parameters of each calorimeter (Table 1) are fixed, except the heat capacity C_1 . The parameters α and β of the external temperatures T_{O1} and T_{O2} functions are also fixed (Eqs. (7), Eq. (8) and Table 3). However, the T_0 values are determined in the measurement.

Fig. 7 shows a measurement performed on the volar wrist area of a healthy 67-year-old male subject. In this experiment, the thermostat temperature was programmed to step from 28 to 31 °C, then from 31 to 34 °C, and finally from 34 to 39 °C, with all steps performed at a 3K/min rate. The figure presents the experimental and calculated calorimetric signal and thermostat temperature, the determined heat flux W_1 and the thermostat power W_2 . After thermal excitation, the skin returns to its initial state. The stepwise changes of the thermostat temperature allow to check that the determined power W_1 also follows a stepwise pattern. Under this assumption, the fitting of the calorimetric signal and thermostat temperature is acceptable. In this measurement, the obtained value of C_1 was 4.7 J/K, and the average value of T_0 was 2.3 °C.

To explain the heat transfer process through the calorimeter, Fig. 8A presents a schematic representation of this mechanism, while Table 4 shows the values of temperatures and heat flows for the measurement

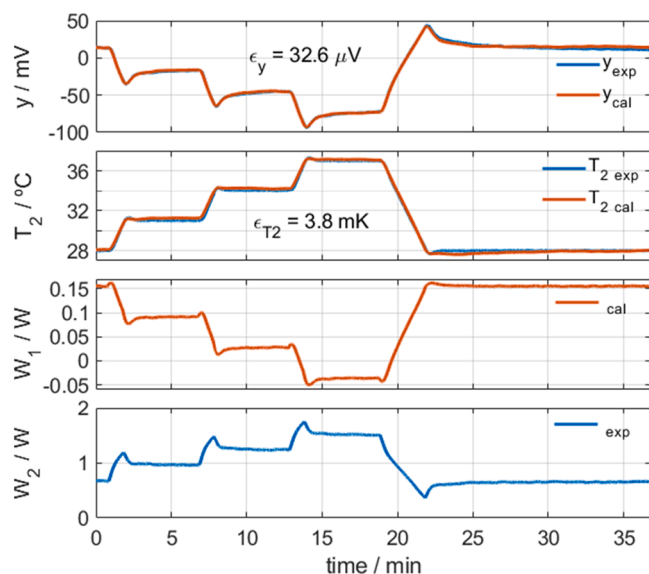


Fig. 7. Measurement performed on the left wrist volar area of a healthy 67-year-old male subject. Calorimetric signal (y), thermostat temperature (T_2), determined skin power W_1 and thermostat power W_2 . Experimental (in blue) and calculated (in red) curves are shown, and RMSE values are indicated. Calorimeter S2, $I_{pel} = 0.1$ A, $np = 2210$, $dt = 1$ s, $T_{room} = 21.2$ °C.

shown in Fig. 7. Initially the thermostat is set at $T_2 = 28$ °C. In this steady-state condition, the heat flux W_1 is outgoing from the human body and is divided into two: one part is transmitted through the measurement thermopile (W_{12}), while the other part is dissipated to the surroundings (W_{10}). At the same time, the power transmitted to the cooling thermopile (W_{20}) is equal to the power dissipated in the

thermostat (W_2) plus the power transmitted through the measuring thermopile (W_{12}). For $T_2 = 31$ °C and $T_2 = 34$ °C, the W_1 heat flux sign remains unchanged, but the sign of the heat flux through the measuring thermopile W_{12} reverses. However, at $T_2 = 37$ °C, both heat fluxes W_1 and W_{12} become negative. These results are consistent with temperatures T_1 , T_{01} , T_2 y T_{02} .

The uncertainty of the determined heat flows depends on the oscillations of the calorimetric signal and the thermostat temperature. For skin measurements, these steady-state oscillations are 1 mV and 15 mK peak-to-peak. As a result, the oscillations of the calculated power W_1 are 4 mW peak-to-peak.

Measurements were also taken with the calorimeter exposed directly to the air, without contact with the calibration base or the skin (Fig. 8B). The thermostat temperature was programmed identically to the previous case (Fig. 7). These measurements allow the determination of the portion of the measured heat capacity, C_1 , that corresponds to the calorimeter itself, and not to the calibration base or the skin.

This offset heat capacity, denoted as C_0 , depends on the intrinsic characteristics of the calorimeter. The calculation process is identical to the one previously described. Fig. 9 shows the calorimetric signal, the experimental and calculated thermostat temperatures, the calculated heat flux W_1 transmitted through the measurement plate, and the experimental power W_2 dissipated in the thermostat. Table 5 shows the heat fluxes for this case. After several repeated measurements, we obtained the C_0 values for each calorimeter:

- Calorimeter S0: $C_0 = 3.07 \pm 0.08$ (J/K)
- Calorimeter S1: $C_0 = 2.31 \pm 0.07$ (J/K)
- Calorimeter S2: $C_0 = 2.31 \pm 0.07$ (J/K)

Note the validity of the sensor operating model in the three cases analyzed: (1) calibration on the base, (2) measurement on the skin, and

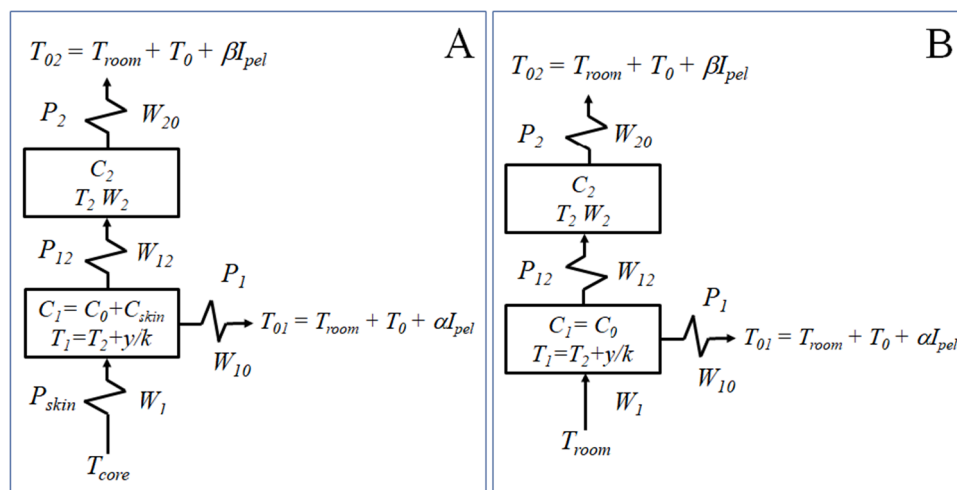


Fig. 8. Illustrative diagram of the heat fluxes A) when the calorimeter is applied to the skin, and B) when the calorimeter measuring plate is directly exposed to the air.

Table 4

Values of temperatures and heat fluxes for the Fig. 7 measurement ($T_{room} = 21.1$ °C, $T_0 = 2.3$ °C, calorimeter S2). The positive sign criteria for W_1 , W_{12} , W_{10} and W_{20} is shown in the diagram Fig. 8. The power dissipated in the thermostat (W_2) is always positive. Temperature is expressed in °C, calorimetric signal in mV, and power in mW.

T_1	T_{01}	T_2	T_{02}	y	W_1	W_{12}	W_{10}	W_2	W_{20}
28.6	25.0	28.0	15.0	13.2	155	51	104	669	720
30.3	25.0	31.0	15.0	-16.7	92	-65	157	959	894
32.0	25.0	34.0	15.0	-45.5	27	-177	204	1235	1058
33.8	25.0	37.0	15.0	-72.3	-37	-282	245	1502	1220
28.5	25.0	28.0	15.0	11.4	155	44	111	660	704

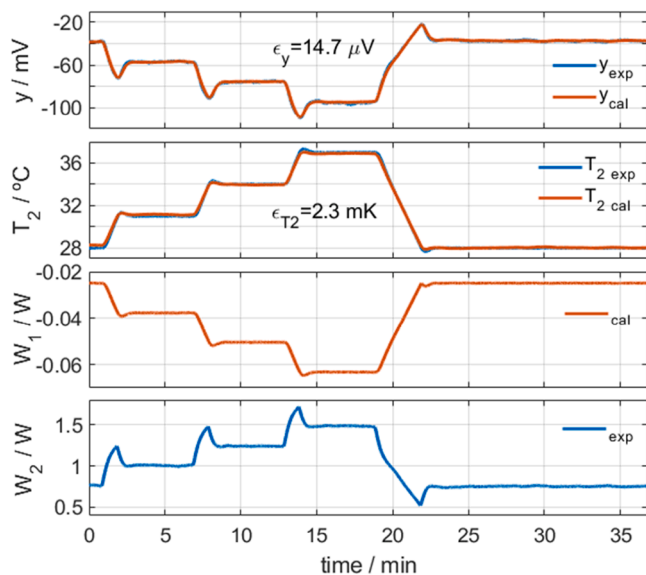


Fig. 9. Measurement performed to determine C_0 , with the calorimeter exposed to the air. Calorimetric signal (y), thermostat temperature (T_2), calculated heat flux (W_1), and thermostat power (W_2). Experimental curves (in blue) and calculated curves (in red) are shown, with RMSE values indicated. Calorimeter $S1$, $I_{pel} = 005$ A, $np = 2210$, $dt = 1$ s, $T_{room} = 21.2$ °C, $C_0 = 2.3$ J/K.

(3) measurement in air.

4.2. Determination of heat capacity and the thermal resistance at rest

When the calorimeter is applied on the skin, the measured heat capacity C_1 includes a volume of skin whose temperature has been modified during the measurement process. The skin heat capacity (C_{skin}) is obtained by subtracting the previously determined offset C_0 from C_1 . The equivalent skin thermal resistance (R_{skin}) is defined as the ratio of the temperature change associated with the heat capacity C_1 to the skin heat flux change W_1 .

$$C_{skin} = C_1 - C_0, R_{skin} = \frac{\Delta T_1}{\Delta W_1} = \frac{\Delta T_2 + \Delta y/k}{\Delta W_1} \quad (10)$$

In this section, measurements were performed on the dorsal and

Table 5

Values of temperatures and heat fluxes for the Fig. 9 measurement, to determine the offset heat capacity C_0 (see diagram Fig. 8B). ($T_{room} = 21.1$ °C, $I_{pel} = 0.05$ A) Positive sign criteria for the heat fluxes W_1 , W_{12} , W_{10} and W_{20} are as shown in the sketch in Fig. 8. The power dissipated in the thermostat (W_2) is always positive. Temperature is expressed in °C, calorimetric signal in mV, and power in mW.

T_1	T_{01}	T_2	T_{02}	y	W_1	W_{12}	W_{10}	W_2	W_{20}
26.4	22.2	28.0	17.5	-38.3	-25	-149	124	762	613
28.6	22.2	31.0	17.5	-56.4	-38	-220	182	999	779
30.8	22.2	34.0	17.5	-75.3	-50	-294	244	1240	946
33.0	22.2	37.0	17.5	-94.9	-63	-370	307	1480	1110



Fig. 10. Calorimeters $S0$ and $S1$ placed on the dorsal and volar areas of the wrist.

volar wrist areas of a healthy 30-year-old male subject (Fig. 10), with a thermostat temperature from 28 to 37 °C ($\Delta T_2 = 9$ °C).

Fig. 11 shows the experimental signals of the volar wrist measurement: calorimetric signal y , thermostat temperature T_2 and dissipated power W_2 . The calculated curves are the temperature T_1 , which is determined with the expression $T_1 = T_2 + y/k$ and the heat flux W_1 , which is determined with Eq. (9) and the calorimetric model. Table 6 shows the ambient temperature (T_{room}) and relative humidity (HR %) for each measurement. The table also includes the obtained skin heat capacity (C_{skin}), the power W_{10} and its variation ΔW_1 (see Fig. 11). The heat flux W_1 depends on the ambient temperature and on the subject's thermal state, which is primarily characterized by the core temperature in the measured zone (T_{core}), the equivalent thermal resistance of the skin (R_{skin}), and its heat capacity (C_{skin}). The core temperature in the measurement zone can be determined by the expression:

$$T_{core} = T_1 + W_1 R_{skin} = T_2 + y/k + W_1 R_{skin} \quad (11)$$

As we can see, the heat capacities are 2.3 J/K for the dorsal area and 1.8 J/K for the volar area. However, the thermal resistance ranges from 33 ± 4 K/W in the dorsal area and 24 ± 2 K/W in the volar area. These results correspond to a 4 cm² area, and are specific to that region of the skin. These results appear to be independent of core, ambient and thermostat temperatures, as expected, which is consistent with previous works performed at rest and at normal conditions [27–29]. However, these results may change if the skin exhibits a pathology [30,31], during exercise [28], or under an induced cooling [26,27]. For example, in Table 6, two measurements exhibit an abnormally low core temperature, which is consistent with the subject's reported sensation of cooling.

5. Final discussion

This section focuses on the application of the calorimeter–skin model equations and the assumptions considered for each use case. Two scenarios are distinguished: the subject at rest, and during physical exercise.

In the first case (at rest) we assume that the internal temperature (T_{core}) remains constant, and the heat flux from the skin to the calorimeter's measurement plate (W_1) varies with thermostat temperature, according to Eq. (9). Under these assumptions, the internal thermal resistance is defined by Eq. (10). Once this resistance is known, the internal skin temperature can be determined using Eq. (11). In these conditions, a thermostat temperature change is programmed, and the

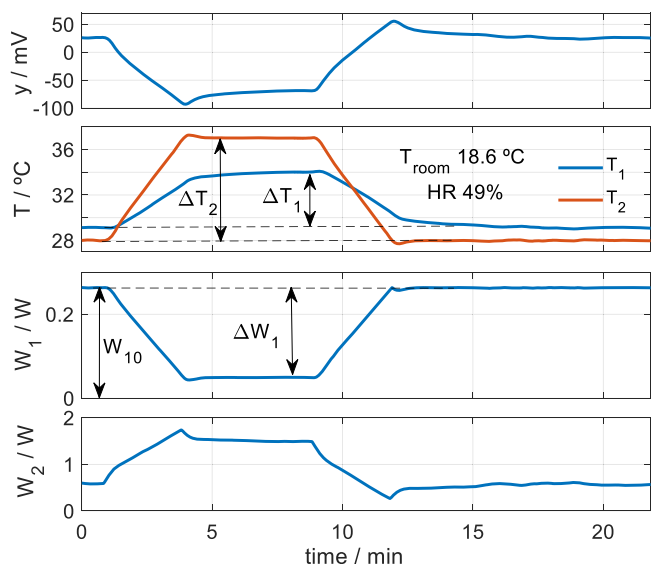


Fig. 11. Calorimetric signal (y), temperatures T_1 and T_2 , and powers W_1 and W_2 , from a measurement performed on the volar wrist area of a healthy 30-year-old male subject at rest, using the S2 calorimeter.

values C_1 and W_1 are obtained. Finally, W_1 is used to calculate the internal thermal resistance of the skin. The heat capacity C_1 depends on the thermal penetration depth, which depends on the duration of the heating cycle. To ensure that the measurements are comparable, we always use the same timing protocol: the thermostat temperature is held at the modified value for 5 min and then returned to its original value over 10 min. According to previous studies [12], this protocol allows us to reach approximately 80 % of the maximum measurable value of C_1 . However, since C_1 only affects the transient state and not the steady state, and because the internal thermal resistance of the skin is determined from steady state values, the estimation of the internal temperature remains reliable.

Regarding uncertainty, we identify three main sources: instrumental, contact-related (between the calorimeter and the skin), and biological variability. The first has been assessed based on the fluctuations in the calorimetric signal and the temperatures involved in the model equations. An analysis of these variables under steady-state conditions yields uncertainties of ± 2 mW in the heat fluxes and ± 1 K/W in the thermal resistance. As for the calorimeter–skin contact, the use of any intermediate paste is not recommended. After disinfecting the contact surfaces, good thermal contact must be ensured through an appropriate fixation. No pressure greater than that of a standard medical bandage is needed. However, during physical activity, the fixation must be firm enough to prevent any relative movement between the skin and the calorimeter. Finally, since the human body is not a static system, the subject's physiological state affects the results. This variability is precisely what the method aims to capture and analyze, in order to define the normal range of values for the measured parameters.

In the second application case, the subject is performing physical

exercise. In this situation, the thermostat of the calorimeter is maintained at a constant temperature. The main assumptions are that the variation in the body's heat flux is caused by changes in the internal temperature, and that the internal thermal resistance remains constant. Of course, the constancy of the internal resistance of the skin cannot be guaranteed, but by performing measurements at rest before and after exercise, an average value for the thermal resistance can be considered. Under these assumptions, and with T_2 held constant, the skin–calorimeter model equation is as follows:

$$T_{core}P_{skin} = \frac{C_1}{k} \frac{dy}{dt} + \frac{P_1 + P_{12} + P_{skin}}{k} y + (P_1 + P_{skin})T_2 - P_1(T_{room} + T_0 + \alpha I_{pel})$$

$$W_2 = -\frac{P_{12}}{k} y + C_2 \frac{dT_2}{dt} + P_2 T_2 - P_2(T_{room} + T_0 + \beta I_{pel})$$
(12)

The conductance P_{skin} is the inverse of the thermal resistance ($P_{skin} = 1/R_{skin}$). The ambient temperature T_{room} is measured with a specific sensor, and its local increase near the calorimeter (T_0) is determined using a second equation (Eq. (12)) in which all parameters and variables are known. Using the model equations, we simulated this exercise scenario considering $R_{skin} = 25$ K/W, and an initial internal temperature of $T_{core} = 33$ °C, which increases exponentially by 3.5 °C with a time constant of 4 min. After exercise, the return to baseline is modeled with the same time constant. The values used in simulation were: $T_2 = 35$ °C, $T_{room} = 24$ °C, $T_0 = 2.5$ °C, $I_{pel} = 0.1$ A, and a heat capacity $C_1 = 6$ J/K. These values are based on a preliminary study involving a subject during physical activity [3]. Fig. 12 shows both the simulated core temperature and the reconstructed one, calculated using Eqs. 12 and Eq. (13). In Eq. 13, the heat capacity C_1 is not considered. The comparison shows that the reconstruction without C_1 is still close to the nominal value. This confirms that the uncertainty in C_1 has a limited effect on the estimation

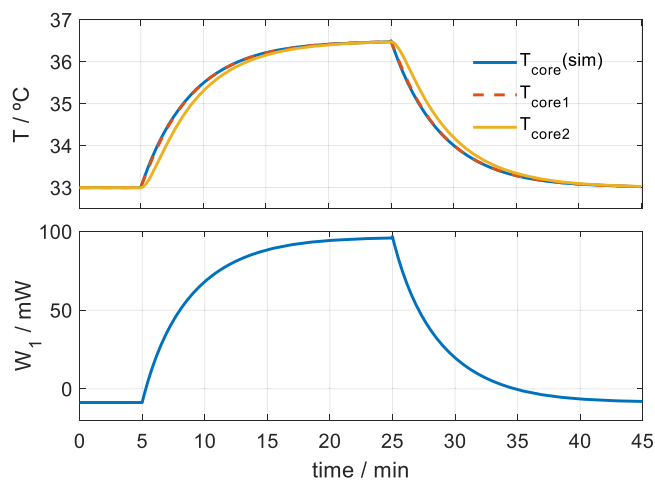


Fig. 12. Simulation of the skin heat flux (W_1) and the internal temperature (T_{core}) for a subject performing exercise. Thermostat temperature was set to 35 °C and ambient temperature T_{room} to 24 °C. Both the simulated T_{core} and the values reconstructed using by Eqs. (12) (T_{core1}) and Eq. (13) are shown (T_{core2}).

Table 6

Results of measurements performed on the dorsal (D) and volar (V) wrist areas of a healthy 30-year-old male subject at rest (seated). The three calorimeters (S0, S1, and S2) were used. The thermostat temperature programming was the same for all measurements and is represented in Fig. 11 ($\Delta T_2 = 9$ °C).

Calorimeter	$T_{room}/$ °C	HR %	$T_{core}/$ °C	$\Delta T_1/K$	W_{10}/W	$\Delta W_1/W$	C_{skin} J/K	R_{skin} K/W
S0 – D	19.0	48	37.1	6.1	0.196	0.163	2.3	37.4
S0 – V	19.2	48	36.3	5.8	0.235	0.227	1.8	25.7
S1 – D*	19.6	53	32.2	5.4	0.144	0.175	2.3	30.8
S2 – D*	19.6	53	30.6	5.3	0.109	0.181	2.4	29.4
S1 – V	18.6	49	35.6	5.1	0.267	0.205	1.8	24.7
S2 – V	18.6	49	35.1	4.9	0.264	0.214	1.8	22.7

* In these measurements, the subject experienced a sensation of cold.

of the internal temperature.

$$T_{core} = \frac{P_1 + P_{12} + P_{skin}}{kP_{skin}} y + \frac{(P_1 + P_{skin})}{P_{skin}} T_2 - \frac{P_1}{P_{skin}} (T_0 + T_{room} + \alpha I_{pet}) \quad (13)$$

Fig. 12 also shows the heat flux, which depends on T_{room} , T_2 , and I_{pet} . However, if these conditions remain constant during the measurement, changes in heat flux reflect changes in internal temperature. This section highlights the need for additional measurement campaigns involving different subjects and various conditions of rest and moderate to intense physical activity, in order to define the normal range of internal thermal resistance values and internal temperature variations.

6. Conclusions

In this work, a calibration procedure and a calorimetric model were developed and validated for the thermal characterization of the skin using non-differential heat conduction calorimeters. Unlike conventional differential calorimeters, the variability of ambient and thermostat temperatures affects the measurements, requiring a specific modeling approach to correct these effects.

- (1) A full calibration of three non-differential skin calorimeters has been performed, incorporating the effects of ambient temperature and the cooling system on the calorimeter. The calibration enables the determination of the heat flux transmitted through the instrument without requiring baseline correction. The calorimeter's operating model obtained has been successfully applied in electrical calibrations, skin measurements and measurements with the calorimeter applied directly to the air (with no sample).
- (2) The operating model and electrical calibration were validated by measuring the thermal properties of the skin (heat capacity and thermal resistance) in the dorsal and volar areas of the wrist of a subject at rest using three different skin calorimeters. The results obtained were similar and consistent with previous works.
- (3) Additionally, a key innovation of this work is the incorporation of the skin into the calorimetric model. This advancement allows the measured heat flux to be decomposed into its components and enables the estimation of the core temperature of the tissue where the measurement is performed. This feature enhances the utility of the calorimeter.
- (4) This non-invasive instrument is of great interest for studying human physiology in both resting and exercising subjects. It is capable of measuring the heat capacity, the thermal resistance of the skin, the heat flux and the internal temperature of the human body at the measurement location ($2 \times 2 \text{ cm}^2$). Additionally, the device can be integrated into multi-sensor instruments for monitoring human exercise.

Ethics statement

The study was conducted in accordance with the Declaration of Helsinki, and approved by the Human Experimentation Ethical Committee of the University of las Palmas de Gran Canaria, (protocol CEIH-2024-02, approved on April 2024).

Funding

This research was funded by the Government of the Canary Islands through the "Convocatoria 2024 de Subvenciones para la realización de Proyectos de I + D Aplicada (Modalidad B), en el marco de la Estrategia de Especialización Inteligente de Canarias RIS-3 Ampliada, y cofinanciado por el Fondo Europeo de Desarrollo Regional (FEDER) 2021–2027" Project: "Monitorización de la capacidad calorífica y la resistencia térmica de la piel mediante un calorímetro de piel (SKIN-CAL)" ID: ProID2024010002.

CRedit authorship contribution statement

Pedro Jesús Rodríguez de Rivera: Writing – original draft, Validation, Project administration, Methodology, Data curation, Conceptualization. **Miriam Rodríguez de Rivera:** Visualization, Validation, Methodology, Investigation, Conceptualization. **Fabiola Socorro:** Writing – review & editing, Validation, Supervision, Resources. **Manuel Rodríguez de Rivera:** Writing – review & editing, Software, Formal analysis, Data curation, Conceptualization.

Declaration of competing interest

The authors declare that they have no known competing financial interests or personal relationships that could have appeared to influence the work reported in this paper.

Data availability

Data will be made available on request.

References

- [1] P.K. Gallagher, *Handbook of Thermal Analysis and Calorimetry. Recent Advances, Techniques and Applications*, 5, Elsevier BV., The Netherlands, 2008.
- [2] L.D. Hansen, Toward a standard nomenclature for calorimetry, *Thermochim. Acta* 371 (2001) 19–22, [https://doi.org/10.1016/S0040-6031\(01\)00422-1](https://doi.org/10.1016/S0040-6031(01)00422-1).
- [3] M. Rodríguez de Rivera, et al., New, optimized skin calorimeter version for measuring thermal responses of localized skin areas during physical activity, *Sensors* 24 (18) (2024) 5927, <https://doi.org/10.3390/s24185927>.
- [4] Q.G. Wang, T.H. Lee, C. Lin, *Transfer function modelling. Relay Feedback*, Springer, London, 2003, https://doi.org/10.1007/978-1-4471-0041-6_7.
- [5] W. Zielonkiewicz, Calorimetric models, *J. Therm. Anal. Calorim.* 33 (1988) 7–13, <https://doi.org/10.1007/BF01914579>.
- [6] F. Socorro, M. Rodríguez de Rivera, C.H. Jesús, A thermal model of a flow calorimeter, *J. Therm. Anal. Calorim.* 64 (2001) 357–366, <https://doi.org/10.1023/A:1011582306796>.
- [7] M. Rodríguez de Rivera, F. Socorro, Baseline changes in an isothermal titration microcalorimeter, *J. Therm. Anal. Calorim.* 80 (2005) 769–773, <https://doi.org/10.1007/s10973-005-0727-1>.
- [8] H.S. Carslaw, J.C. Jaeger, *Conduction of Heat In Solids* (1989).
- [9] J.Zhao Jennifer, et al., A two level finite difference scheme for one dimensional Pennes' bioheat equation, *Appl. Math. Comput.* 171 (1) (2005) 320–331, <https://doi.org/10.1016/j.amc.2005.01.052>.
- [10] Lifan Yuan, Jianlin Yu, Suxin Qian, Revisiting thermal penetration depth for caloric cooling system, *Appl. Therm. Eng.* 178 (2020) 115605, <https://doi.org/10.1016/j.applthermaleng.2020.115605>.
- [11] A. Isalgúe, J.L. Pelegrina, V. Torra, Non-differential conduction calorimeter, a tool to study the after quench behaviour in shape memory alloys, *J. Therm. Anal. Calorim.* 53 (1998) 671–683, <https://doi.org/10.1023/A:1010186621841>.
- [12] P.J. Rodríguez de Rivera, M. Rodríguez de Rivera, F. Socorro, M. Rodríguez de Rivera, Validation of a skin calorimeter to determine the heat capacity and the thermal resistance of the skin, *Sensors* 23 (2023) 4391, <https://doi.org/10.3390/s23094391>.
- [13] P.J. Rodríguez de Rivera, M. Rodríguez de Rivera, F. Socorro, M. Rodríguez de Rivera, Monitoring of some minor human skin lesions using a skin calorimeter, *J. Therm. Anal. Calorim.* 149 (2024) 5257–5264, <https://doi.org/10.1007/s10973-024-13204-6>.
- [14] Thermoelectric coolers, <https://lairdthermal.com/products/thermoelectric-cooler-modules>, 2025, (accessed 12 march 2025).
- [15] Omega products, <https://www.omega.co.uk/products.html>, 2025, (accessed 12 march 2025).
- [16] V.M. Alfaro, PID controllers' fragility, *ISA Trans.* 46 (2007) 555–559, <https://doi.org/10.1016/j.isatra.2007.03.006>.
- [17] J.A. Nelder, R. Mead, A simplex method for function minimization, *Comput. J.* 7 (1965) 308–313, <https://doi.org/10.1093/comjnl/7.4.308>.
- [18] J.C. Lagarias, J.A. Reeds, M.H. Wright, P.E. Wright, Convergence properties of the Nelder-Mead simplex method in low dimensions, *SIAM J. Optim.* 9 (1998) 112–147, <https://doi.org/10.1137/S1052623496303470>.
- [19] Fminsearch function, <https://es.mathworks.com/help/matlab/ref/fminsearch.html>, 2025, (accessed 13 march 2025).
- [20] R. Sabbah, An Xu-wu, et al., Reference materials for calorimetry and differential thermal analysis, *Thermochim. Acta* 331 (2) (1999) 93–204, [https://doi.org/10.1016/S0040-6031\(99\)00009-X](https://doi.org/10.1016/S0040-6031(99)00009-X).
- [21] K. Parsons, *Human Thermal Environments: The Effects of Hot, Moderate, and Cold Environments on Human Health, Comfort and Performance*, 2nd Edition, CRC Press, 2002, <https://doi.org/10.1201/9781420025248>.
- [22] M. Gleeson, Temperature regulation during exercise, *Int. J. Sports Med.* 2 (19 Suppl) (1998) S96–S99, <https://doi.org/10.1055/s-2007-971967>.

- [23] J.L. Taylor, J. Myers, A.R. Bonikowske, Practical guidelines for exercise prescription in patients with chronic heart failure, *Heart Fail. Rev.* 28 (6) (2023) 1285–1296, <https://doi.org/10.1007/s10741-023-10310-9>.
- [24] A. Keijzer, M. Woerlee, B.D. Kluver, M. Buist, Direct measurement of sensible heat transfer between man and his environment, *J. Appl. Physiol.* 33 (1972) 677–680, <https://doi.org/10.1152/jappl.1972.33.5.677>.
- [25] H. Anttonen, K. Puhakka, J. Niskanen, P. Ryhänen, Cutaneous heat loss in children during anaesthesia, *Br. J. Anaesthesia* 74 (1995) 306–310, <https://doi.org/10.1093/bja/74.3.306>.
- [26] J.R. House, M.J. Tipton, Using skin temperature gradients or heat flux measurements to determine thresholds of vasoconstriction and vasodilatation, *Eur. J. Appl. Physiol.* 88 (2002) 141–145, <https://doi.org/10.1007/s00421-002-0692-3>.
- [27] Z. Ostrowski, Modelling and validation of transient heat transfer processes in human skin undergoing local cooling, *Przełąd Elektrotechniczny* 1 (2015) 78–81, <https://doi.org/10.15199/48.2015.05.20>.
- [28] X. Xu, A.J. Karis, et al., Relationship between core temperature, skin temperature, and heat flux during exercise in heat, *Eur. J. Appl. Physiol.* 113 (2013) 2381–2389, <https://doi.org/10.1007/s00421-013-2674-z>.
- [29] P. Eggenberger, et al., Prediction of core body temperature based on skin temperature, heat flux, and heart rate under different exercise and clothing conditions in the heat, *Front. Physiol.* 9 (2018) 1780, <https://doi.org/10.3389/fphys.2018.01780>.
- [30] P.J. Rodríguez de Rivera, M. Rodríguez de Rivera, F. Socorro, M. Rodríguez de Rivera, Calibration and operation improvements of a calorimetric sensor for medical applications, *Measurement* 186 (2021) 110134, <https://doi.org/10.1016/j.measurement.2021.110134>.
- [31] T. Okabe, et al., First-in-human clinical study of novel technique to diagnose malignant melanoma via thermal conductivity measurements, *Sci. Rep.* 9 (2019) 3853, <https://doi.org/10.1038/s41598-019-40444-6>.